Powder Technology 353 (2019) 450–458

Contents lists available at ScienceDirect

Powder Technology

journal homepage: www.elsevier.com/locate/powtec

Utilization of waste coconut shells in the reduction roasting of overburden from iron ore mines

Deepak Nayak, Nilima Dash, Nigamananda Ray, Swagat S. Rath *

CSIR-Institute of Minerals and Materials Technology, Bhubaneswar, Odisha 751013, India

ARTICLE INFO

Article history:
Received 6 September 2018
Received in revised form 14 February 2019
Accepted 22 May 2019
Available online 24 May 2019

Keywords:
Iron ore overburden
Coconut shell
Reduction roasting
Biomass

ABSTRACT

The reduction of iron ore using biomass-based reductants has opened up a new chapter because of its contribution to energy conservation and emission reduction. In this connection, the application of waste coconut shells (CS) as the reductant in the reduction roasting-magnetic separation of an iron ore overburden sample is explored. Characterization studies on the overburden having 49% Fe suggest that the sample is mostly a goethitic ore containing kaolinite as the major gangue mineral. A concentrate with 63.2% Fe at an iron recovery of 66.2% has been obtained from the low-intensity magnetic separation of the overburden roasted at a temperature of 800 °C, time of 60 min and a CS to feed ratio of 0.2. Characterization studies indicate the formation of magnetite and hematite under these optimum conditions, whereas roasting at a temperature of 900 °C and a reductant to feed ratio of 0.3 is found to form feebly magnetic phases like wustite, fayalite and complex iron aluminosilicates resulting in poor iron recovery. The thermo-gravimetric analysis studies explain the disintegration of the biomass and reduction of the iron ore thereby validating the reduction sequence as predicted using the characterization studies.

1. Introduction

The economic and social development of India largely depends on minerals and metals, but their exploration; excavation and processing generate vast amounts of wastes in the form of overburden, tailings, mine water, slags, etc. Most of these residues containing essential useful minerals are ignored by industries and are dumped in nearby areas. Keeping in view the rising demand for iron and steel in India, fresh exploration of iron ore resources, and thereby generation of mining wastes is on the anvil. Iron ore overburden, which is generated during selective mining, is one of such low-grade iron resources which cannot be directly subjected to iron making because of the low iron content. Therefore, it is essential to develop beneficiation strategies in order to upgrade its iron content. As the mineralogical characteristics of the iron ore overburden differ from site to site, the beneficiation strategies to be adopted have to be unique for each of them [1]. In general, the overburden in Indian iron ore mines is highly weathered and mostly rich in goethite. Goethite, due to its adsorption capacity can incorporate other elements like Al, Si, Mn, P, etc. in the crystal structure during its formation [2]. It is this characteristic of goethite for which beneficiation of the majority of the overburden is inevitable before use in iron making. However, many of these low-grade iron ore resources do not respond to physical beneficiation operations such as classification, gravity concentration, magnetic separation, and flotation. This may be attributed to the complex association of the mineral phases leading to a poor liberation pattern. In such cases, reduction roasting is getting attention as an alternative beneficiation strategy, where the goethite and hematite values are reduced to magnetite and easily recovered using a low-intensity magnetic separation unit. Recently, the coupled approach of reduction roasting and magnetic separation has been proved to bring in good iron grades and recoveries from some poorly liberated iron ores [3–5]. Hence, it is high time to study all the pros and cons of the process of reduction roasting and establish it on the commercial scale.

Coal and coke are the established reductants for iron ores. However, it has become crucial to look for a way forward to the development of alternative reductants considering the fast depletion of high-grade coal reserves. In this connection, waste biomass is now being considered as an alternative reductant. It is well-established by many researchers that biomass is feasible for the replacement of fossil fuels such as coal, coke and natural gases, as a non-toxic and renewable solid fuel [6–8]. Biomass is an organic matter, wherein solar energy is stored in chemical bonds. The stored chemical energy releases when the bonds between the adjacent carbon, hydrogen, and oxygen molecules get broken by digestion, combustion, or decomposition [9]. Secondly, various hydrocarbon gases and solid carbon generated by pyrolysis of biomass can be utilized in iron-making [10,11]. Besides, the use of agricultural and industrial biomass residues would help in the disposal of the same. For this reason, several studies have been carried out on iron oxide

* Corresponding author.
E-mail address: ssrath@immt.res.in (S.S. Rath).

https://doi.org/10.1016/j.powtec.2019.05.053
0032-5910/

reduction using biomass. For instance, Yong-bin et al. [12] studied the reductive magnetic roasting of limonite both by coal and biomass. Biomass was found a better reductant than coal since the required roasting temperature was lower than over 100 °C. Pine sawdust as a biomass fuel in magnetization of goethite ore was evaluated by Wu et al. [13] while Abd Rashid et al. [14] utilized palm kernel shell waste for the reduction of a Malaysian iron ore. The magnetization of goethite ore from China by pine, rice chaff, and corn straw biomass fuels has also been examined [15]. Similarly, briquettes made up of vegetative remains have been established as reductants in the roast-reduction of iron ore slimes [16].

Vast quantities of the agricultural wastes generated in many of the developing countries are mostly used as fuel. Coconut shell is one such agricultural solid waste that can be regarded as a fuel. According to the sources from Department of Agriculture and Cooperation, Ministry of Agriculture, Government of India; India is the third leading coconut producers in the world, with an annual production of ~22 billion nuts in 2016 [17]. The overall production of coconut is rising every year since the last decade and is expected to increase further with the increasing global demand. It will lead to the generation of a massive amount of coconut shells, causing disposal problems. Therefore, there is a need for proper utilization of the available agricultural waste from the coconut industries. Many researchers found coconut shells to be useful for the production of activated carbons [18,19]. Coconut shells can also find takers from the construction industries as they can be readily used in concrete [20]. However, there are no reports on the usage of coconut shell as a reductant in the processing of iron ores. Notably, in India, where abundant agricultural wastes are discharged every day, coconut shell can be thought of being a potential reductant in iron making.

In light of the above discussions, the authors have attempted to utilize coconut shells as the reductant in the reduction roasting-magnetic separation of iron ore overburden to produce a high-grade iron ore concentrate. Also, the microstructural changes, phase transformations, and thermal behaviour during the roasting of the iron ore by coconut shells have been looked into.

2. Materials and methods

2.1. Material characterization

Iron ore overburden sample was collected from one of the mines in Jharkhand, India. Coconut shells (CS) received from the nearby areas of Bhubaneswar, India were used as the reductant. Both the iron ore and CS were crushed to below 10 mm and riffled to produce representative samples.

A representative sample of the ore was subjected to chemical analysis, optical microscopy (reflected light microscopy), X-ray Diffraction (XRD), X-ray Fluorescence (XRF) spectroscopy and Thermogravimetric Analysis (TGA) while characterization studies like Fourier Transform Infrared Spectroscopy (FTIR), TGA and proximate analysis were undertaken for CS. Optical microscopic studies of the feed iron ore samples were carried out in a Leitz instrument using the polished section of the ore samples. XRD (PANalytical, X'Pert PRO) was performed in the range of 10–80 °C with a scanning speed of 1°/min. XRF analysis was carried out in a PANalytical (Model-Zetium 4.0 kW) instrument using WROXI standard. PamTGA (Netzsch Sta 449C) of both iron ore and biomass was conducted up to 1000 °C with 10 °C/min heating rate in argon gas. FTIR studies were performed using a Shimadzu instrument in the range of 400–4000 cm^{-1} over KBr disc pellets. The proximate analysis and gross calorific value (GCV) were determined in a Leco make thermogravimetric analyzer and a bomb calorimeter, respectively. Scanning Electron Microscopy coupled with Energy Dispersive X-ray Spectroscopy (SEM-EDS) studies on some of the roasted products were carried out using a ZEISS EVO instrument for understanding the transformation of different mineral phases during reduction roasting. XRD studies of the roasted products were also undertaken to ascertain the phase changes of the minerals.

2.2. Reduction roasting and magnetic separation

The roasting studies were carried out using a laboratory muffle furnace. The overburden and CS were crushed to −10 mm size and used in the roasting experiments. For each test, 150 g of the ore sample was mixed with CS in the desired reductant to feed ratio and kept in a refractory crucible inside the furnace. After roasting, the samples were cooled to room temperature by water quenching to avoid re-oxidation. The roasted samples were ground to -75 μm and subjected to magnetic separation tests in a Low-Intensity Magnetic Separation (LIMS) unit having a magnetic intensity of ~0.18 T. The magnetic and non-magnetic parts were collected separately, dried and then analyzed for iron content by dissolution in hydrochloric acid followed by the standard dichromatic titration method.

3. Results and discussion

3.1. Materials characterization

3.1.1. Iron ore characterization

The results of the wet chemical analysis of the bulk sample along with the four size fractions are depicted in Fig. 1. The raw sample contains 49.02% Fe, 10.2% Al_2O_3, 7.32% SiO_2 and 12.04% LOI. The figure also shows that the coarser size fractions (+1 mm) have relatively uniform levels of Fe, Al_2O_3, and SiO_2, whereas the fine particles contain more impurities and are a little less in Fe content.

The detailed composition of the bulk ore as determined from XRF spectroscopy is presented in Table 1. It is observed that iron oxide, silica and alumina are the major components of the ore. The Fe (Total) content of 48.5% can be attributed to hematite and goethite. The high LOI content of 11.92% further confirms the presence of goethite as the major mineral. Similarly, the silica and alumina content along with the high LOI content are indicative of the presence of kaolinite phase. The data also suggest that other components are found in traces. Optical microscopic analysis of the feed sample was further carried out to supplement the finding of the chemical analysis.

Optical microscopic studies on the overburden sample as displayed in Fig. 2 show that goethite is the major iron mineral. The modal analysis under a microscope reveals that the sample contains goethite to the tune of ~60%, whereas hematite, clay (mainly kaolinite) and quartz contribute approximately 20%, 15%, and 5%, respectively. The presence of minor to considerable amounts of kaolinite and quartz in association with goethite in the ore is indicative of its low-grade nature. Goethite is found to occur in different forms such as earthy goethite showing colloform texture with cavities often filled with clayey materials, and

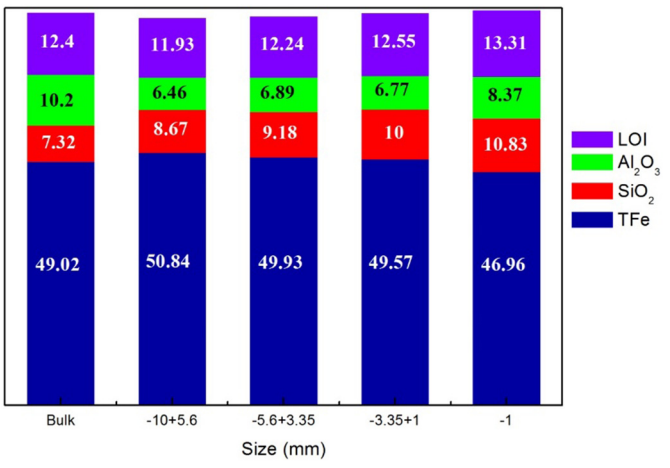

Fig. 1. Result of chemical analysis showing the distribution of Fe, Al_2O_3, SiO_2 and LOI in bulk as well as size fractions of the raw ore sample.

Table 1
XRF analysis of the raw ore sample.

S. No.	Constituent	Wt. (%)	S. No.	Constituent	Wt. (%)
1	SiO_2	7.242	11	V_2O_5	0.056
2	TiO_2	0.329	12	Cr_2O_3	0.049
3	Al_2O_3	10.542	13	ZrO_2	0.005
4	Fe_2O_3	69.355	14	BaO	0.002
5	Mn_3O_4	0.065	15	NiO	0.002
6	MgO	0.021	16	CuO	0.005
7	CaO	0.029	17	ZnO	0.005
8	Na_2O	0.05	18	PbO	0.001
9	K_2O	0.124	19	Fe(T)	48.5
10	P_2O_5	0.053	20	LOI	11.921

ochreous goethite containing pores filled with clay (Fig. 2a). Also, some massive goethite replacing microplaty hematite aggregates are seen. Fig. 2b illustrates vitreous goethite showing segmented twinning with cavities filled with clay and relicts of quartz and subhedral hematite grains. At other places, hematite is found to be present mostly as porous particles infilled with some clay. Clay is also entrapped within the pores of earthy or ochreous goethite. The presence of quartz particles is very less as subhedral shaped grains. The overall mineralogical picture as depicted in Fig. 1 and Fig. 2 suggests that this sample comes under the category of a difficult to treat ore so far as physical beneficiation techniques are concerned.

3.1.2. Biomass characterization

The proximate analysis results of the biomass sample are shown in Table 2. The data reveal that there are a little ash and moisture. While the fixed carbon is about 18%, the volatile content is 73.35% explaining why the GCV is very high.

FTIR spectra undertaken on CS to understand the functional groups of the biomass are shown in Fig. 3. Band shifting around the broad peak at 3390 cm^{-1} reveals the possible involvement of hydroxyl groups [21]. The peaks at 2941 and 2890 cm^{-1} are due to the vibrations of CH, CH_2, and CH_3 groups [22]. The absorption band around 2350 cm^{-1} shows the characteristic of C ≡ C bonds in aromatic rings [23]. The peaks of 1730 cm^{-1} and 1604 cm^{-1} correspond to the aldehyde C═O stretch and alkenyl C═C stretch, respectively [24]. The peak at 1460 cm^{-1} represents the C—H bending of methyl and methylene groups while the one at 1425 cm^{-1} can be attributed to the C—H deformation of lignin [25]. The peak at 1375 cm^{-1} can be assigned to the O—H bending vibrations [22]. The bands at 1250 and 1120 cm^{-1} correspond to acyl and phenyl C—O, whereas the one at 1050 cm^{-1} indicates the presence of the alkoxy C—O [26]. The presence of a peak of 890 cm^{-1} can be attributed to the C—H deformation vibration of cellulose and C—H bending of the syringyl units. Similarly, the peaks at 777 cm^{-1} and others below it indicate the presence of C—H bending [27].

Table 2
Proximate analysis of biomass.

C (%)	Volatile (%)	Ash (%)	Moisture (%)	GCV (KJ/g)
18.19	73.35	1.62	6.84	18.84

3.2. Roasting studies

3.2.1. Effect of reductant and temperature

At first, the roasting studies were carried out by varying the temperature and reductant (CS) content. Six different levels of temperature used in the study were 650 °C, 700 °C, 750 °C, 800 °C, 850 °C, and 900 °C while the reductant to feed ratio was varied between 0.15 and 0.3. The reduction time was fixed at 60 min. The effect of temperature and reductant to feed ratio on iron grade and recovery of the magnetic product is shown in Fig. 4. It is observed that the grade of the iron concentrate increases while recovery decreases with increasing temperature. At the low-temperature regime (650 °C–750 °C), the iron grade decreases with CS addition with a simultaneous increase in the corresponding iron recovery. This might be attributed to the insufficient combustion of the biomass. At temperatures above 800 °C, the grades of all experimental samples having higher biomass are higher than 62%, except for 15% biomass. On the other hand, the iron recoveries of all samples decrease rapidly at temperatures above 800 °C, which may be attributed to the formation of feebly magnetic phases that get collected in the non-magnetic product. It can also be seen at $T = 800$ °C, though the iron recovery at 0.15 reductant to feed ratio is a little bit higher than that with 20% biomass, the grade for the same is poor with 61.73%. In contrast, the grade of the sample with 20% biomass at 800 °C is 63.23% with an iron recovery of 66.24%. Moreover, there is no significant enhancement in the iron grade with further increase in the biomass content or temperature. Therefore, the temperature and reductant to feed ratio at the levels of 800 °C and 0.2, respectively can be considered ideal for producing a suitable iron ore concentrate.

3.2.2. Effect of time

To determine the optimal reduction time, the samples were further roasted at 800 °C and 850 °C for different time intervals varying from 30 min to 90 min, with 0.2 CS to feed ratio. The experimental results are shown in Fig. 5. At $T = 800$ °C, the grade of the concentrate increases up to 60 min and after that remains constant on increasing the time

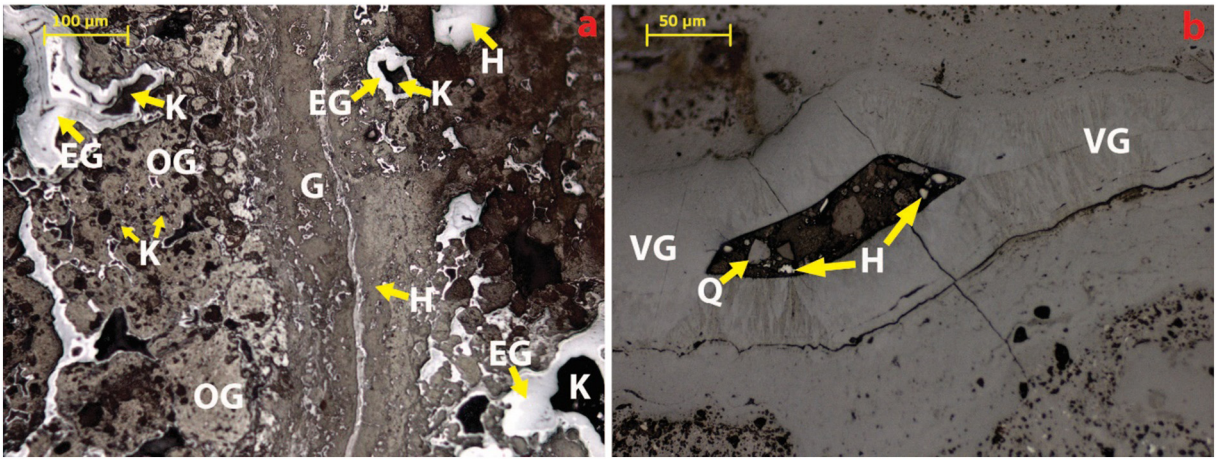

Fig. 2. Mineral phases identified by optical microscopy for the raw iron ore sample. G: Goethite, EG: Earthy Goethite, OG: Ochreous Goethite, VG: Vitreous Goethite, K: Kaolinite, H: Hematite and Q: Quartz.

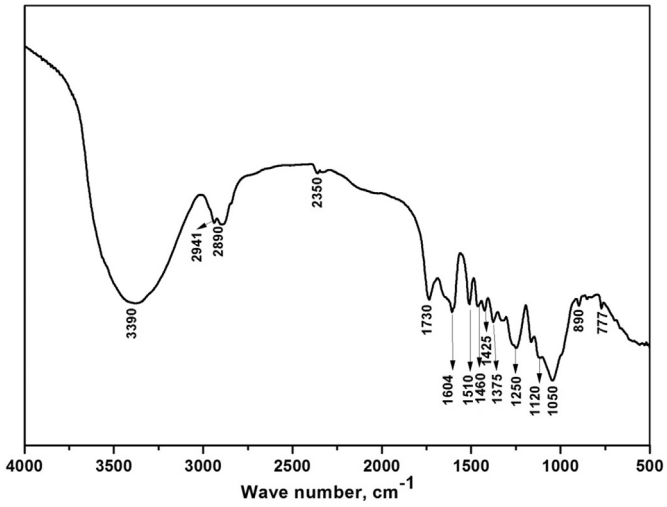

Fig. 3. FTIR spectrum of CS waste.

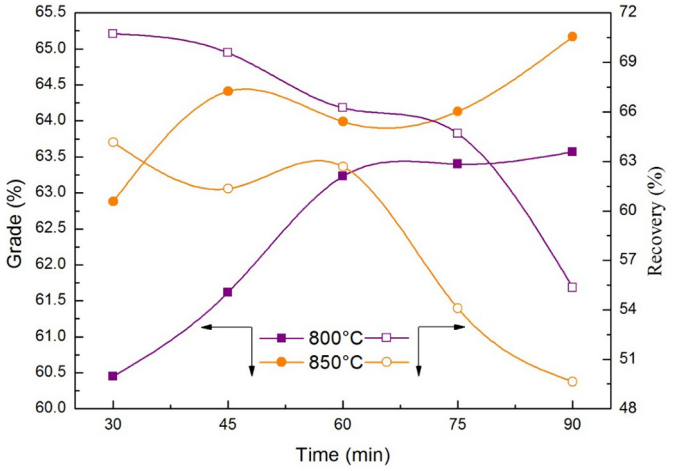

Fig. 5. Effect of roasting time on the grade and recovery of iron in the concentrate at 800 and 850 °C (CS to feed ratio: 0.20).

above 60 min. On the contrary, at $T = 850$ °C, the time has a lesser effect on the grade of the concentrate. It is observed that the iron recovery decreases with an increase in reduction time for both the levels of temperature. However, beyond time periods of 60 min, there is a sharp decrease in the iron recovery at both the temperatures. For example, at 90 min and 850 °C, the grade is found to be 65.17%, though the corresponding iron recovery is as low as 49.65%. It may be due to the over-reduction of the iron oxide phases roasted over a long time resulting in weakly magnetic phases that get separated as a non-magnetic part [28]. Therefore, the optimal reduction time is found to be 60 min.

3.2.3. Effect of particle size

Considering the experimental results as explained above, the optimum parameters for a better grade and recovery obtained are as follows: temperature, 800 °C; time, 60 min; and CS to feed ratio, 0.2. All these experiments were performed with a particle size of −10 mm for both iron ore and biomass. Therefore, a series of experiments were conducted at different particle sizes of both iron ore and biomass to investigate the influence of iron grade and recovery. To begin with, experiments were carried out at four different particle sizes of CS such as −10 + 5.6 mm, −5.6 + 3.35 mm, −3.35 + 1 mm, and − 1 mm; keeping all other optimum parameters constant. Fig. 6 depicts the iron grade and recovery values at four particle sizes of CS. It can be seen that the iron grade remains unaffected while recovery reduces as the particle size decreases. A smaller particle size of the reductant leads to a faster burning rate, and that is why the corresponding degree of reduction is relatively lesser as most of the reducing gases escape the system without causing an effective reduction. In contrast, reducing gases are generated more slowly and steadily from the bigger biomass particles leading to a more efficient reduction; hence, an enhanced iron recovery.

Similarly, tests were done at four different particle sizes of iron ore keeping all other factors at an optimum level. The iron content, as well as recovery, was plotted against ore particle size (Fig. 7). The iron recovery reaches a maximum value at a particle size between 3.35 mm and 1 mm. The fall of iron recovery at finer fractions of iron ore may be attributed to the presence of higher amounts of clay and low Fe content, as depicted in Fig. 1. Still, there is no apparent effect on the grade of the magnetic concentrate by varying the particle size of iron ore. It can be concluded that the change in particle size of both iron ore and biomass has no visible impact on the grade of the concentrate, even though the recovery varies to some extent. Therefore, a particle size of −10 mm is preferable as it helps in maintaining the permeability of the bed.

3.3. Analysis of roasted products

Analysis of roasted products is essential because of their complex dissemination characteristics. It also helps in understanding the

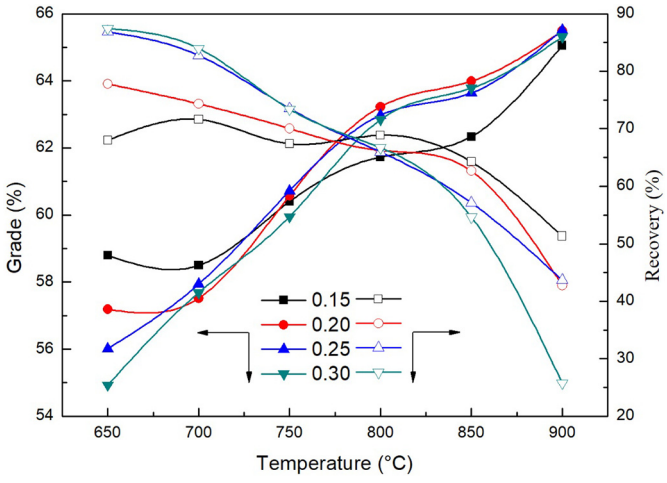

Fig. 4. Effect of roasting temperature and CS to feed ratio on the grade and recovery of iron in the concentrate (roasting time: 60 min).

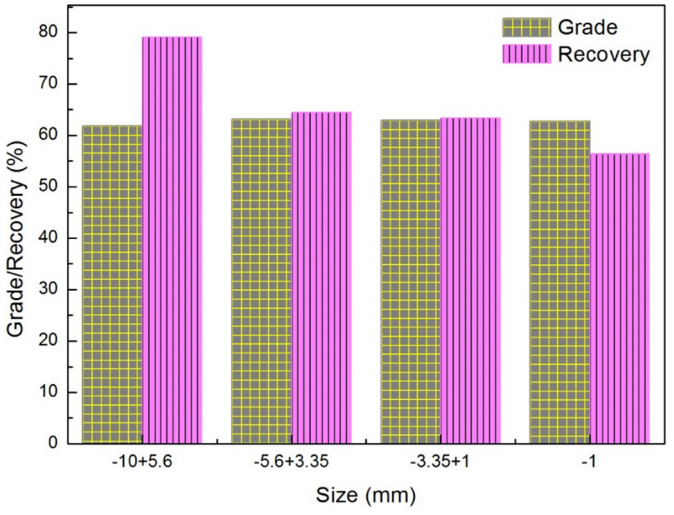

Fig. 6. Effect of particle size of CS on the grade and recovery of iron in the concentrate (roasting temperature: 800 °C, roasting time: 60 min, CS to feed ratio: 0.20).

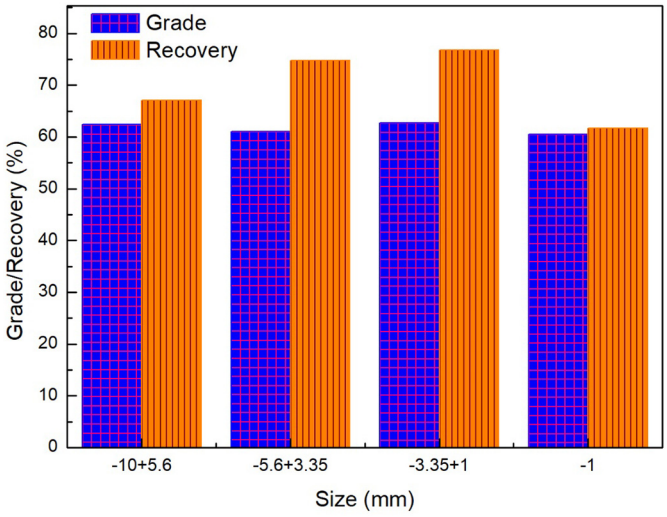

Fig. 7. Effect of particle size of ore overburden on the grade and recovery of iron in the concentrate (roasting temperature: 800 °C, roasting time: 60 min, CS to feed ratio: 0.20).

experimental results as described above. Therefore, reflected light microscopic studies of the roasted product (800 °C, 0.2 CS to feed ratio and 60 min) that led to a magnetic fraction having a Fe grade of 63.2% at an iron recovery of 66.2% were undertaken.

The optical micrograph as shown in Fig. 8 depicts the formation of magnetite as a result of the reduction of the goethite and hematite phases present in the feed. Patches of hematite can also be observed along with magnetite. This hematite has most possibly resulted out of the dehydration and reduction of goethite initially present in the feed ore. Fig. 8a shows the formation of silicate (S) phases along the borders of magnetite (M). The silicate phases appear to be isolated from the iron phases. Several fractures in the sample, both intergranular and transgranular, are observed which can be attributed to the high-temperature treatment. The presence of some unconsumed remnants of biomass (black) can also be seen in Fig. 8b. Overall, the optical micrographs suggest the formation of magnetite accompanied by a better liberation pattern owing to the fractures developed during roasting. This explains why a high-grade magnetic fraction was obtained under these conditions.

Some of the roasting experiments produced a concentrate having a high Fe grade at a very low iron recovery while some others ended up with very low grades of Fe. Therefore, three varieties of roasted products as explained in Table 3 were further analyzed using SEM-EDS. The intention was to understand the effect of the varying roasting conditions

Table 3
Details of roasted products subjected to characterization studies.

Sample nomenclature	Process parameters			Grade (%)	Recovery (%)
	Temperature (°C)	Time (min)	Biomass (%)		
S1	700	60	15	58.5	71.63
S2	800	60	20	63.23	66.24
S3	900	60	30	65.31	25.77

on the formation of different phases. It may be noted that particle size for both the iron ore and CS, to generate the samples S1, S2, and S3, was kept constant at −10 mm.

3.3.1. Electron microscopy analysis

The SEM images of the three different roasted samples namely, S1, S2, and S3 as shown in Fig. 9 highlight the development of various mineral phases under different experimental conditions. The corresponding EDS data represented in triangular plots reveal the distribution of Fe, Al, and Si in different proportions. The reduced ore showed in S1 shows the presence of magnetite, which confirms the reduction of goethite and hematite to magnetite. Hematite can also be observed in this sample which is the result of the dehydration and reduction of goethite present in the feed. However, the presence of magnetite is more pronounced in S2, which represents the product roasted at the optimum levels of parameters. The roasted product (S3) obtained at a temperature of 900 °C, a CS to feed ratio of 0.3 and a time of 60 min shows the formation of phases like wustite (FeO) and silicates such as fayalite (Fe_2SiO_4) along with hematite and magnetite.

The ternary composition plots as shown in Fig. 9 feature the Fe rich phases (containing more than 70% Fe) as green points and phases having lesser Fe percentage as red. The distribution of these points across the triangles depicts the separation of the Fe and gangue phases. On comparison of S1 and S2, it is evident that the later has more Fe-rich points indicating a more efficient reduction of iron phases allowing minimal unwanted reactions of iron with other phases. The ternary composition of S3 reveals the presence of more red points located towards the centre of the triangle. This confirms the formation of complex iron aluminium silicates involving Fe, Al, and Si with almost equal mass percentages.

3.3.2. Phase transformation during reduction

XRD was employed to each of the roasted products (S1, S2, and S3) listed in Table 2 to track changes in mineralogy and confirm the reduction mechanism as observed in SEM-EDS.

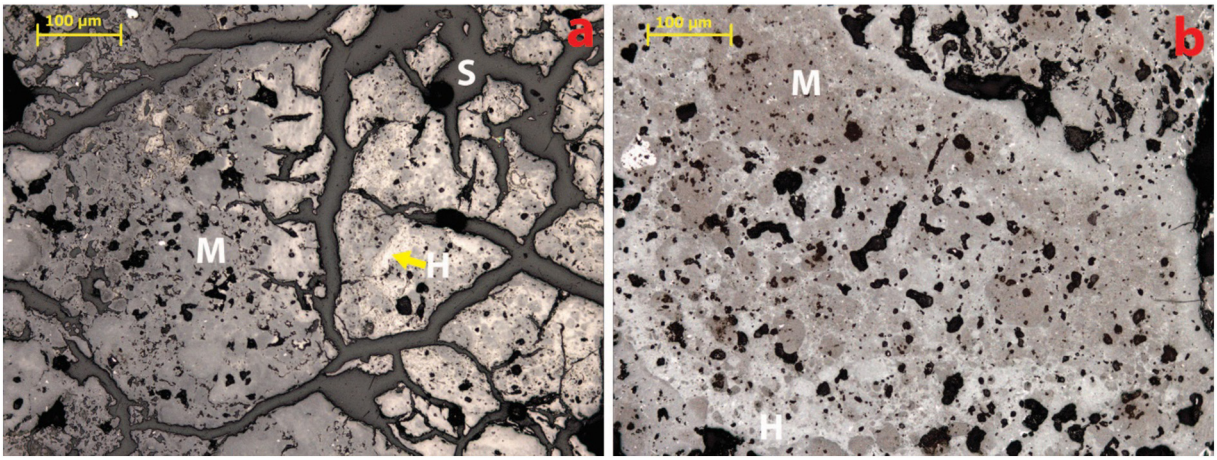

Fig. 8. Reflected light microscopic photograph of the iron ore sample roasted at 800 °C, 0.2 CS to feed ratio and 60 min.

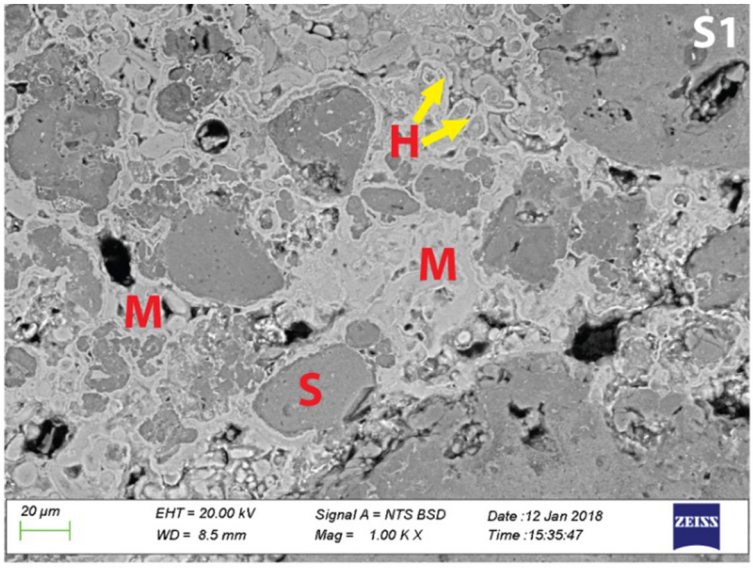

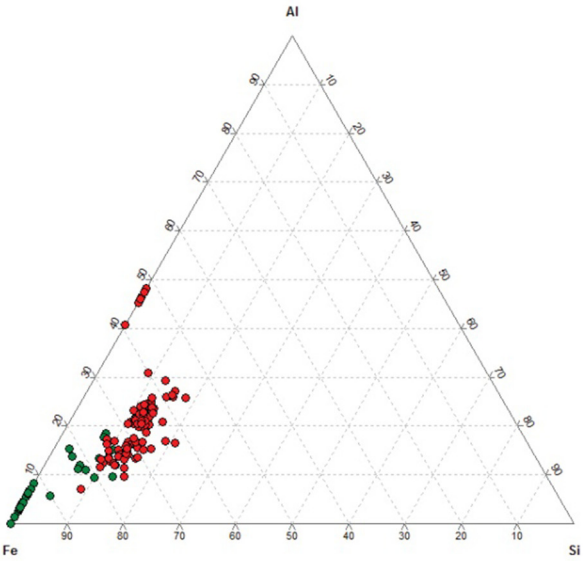

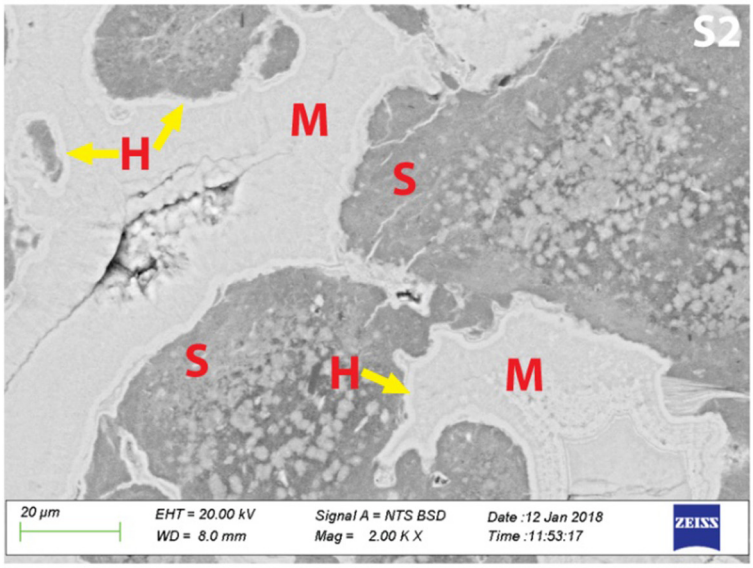

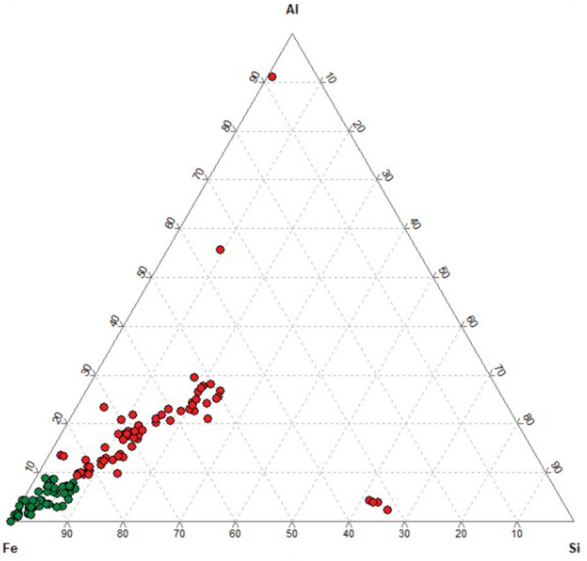

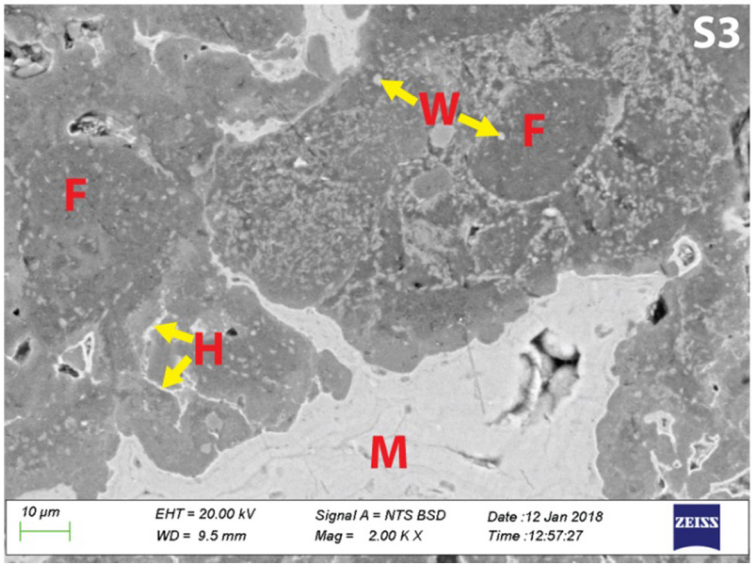

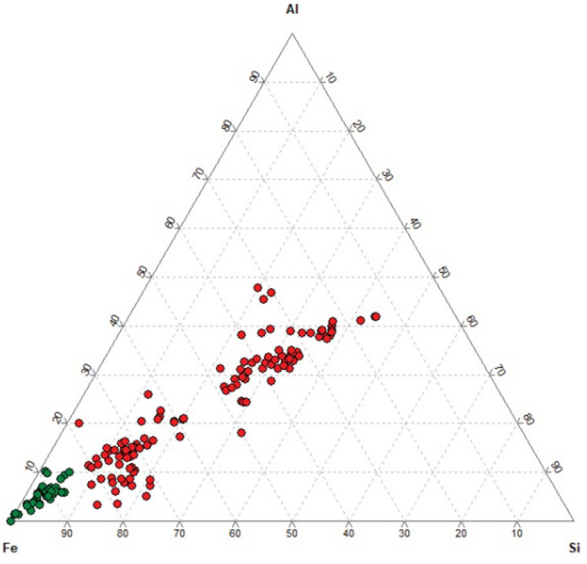

Fig. 9. (Left) BSE images of the roasted samples S1, S2 and S3. (Right) Ternary composition diagrams based on EDS analysis.

In the raw iron ore sample, it is clear that iron exists mainly as goethite and hematite (Fig. 2). On comparing the XRD patterns of the raw ore and the selected roasted products (Fig. 10), it is apparent that goethite and hematite have mostly converted to magnetite. In the ore roasted at 700 °C (sample S1), hematite still exists indicating that the complete reduction to magnetite has not occurred at this temperature, time and biomass content. However, in the case of sample S2, the peaks of hematite are less intense than those in S1. In contrast, the intensities of magnetite peaks have increased. This infers that 800 °C, 60 min, and 0.2 CS to feed are suitable conditions for reduction to magnetite. It is also noticed that peaks of wustite, fayalite, and hercynite along with magnetite are present in sample S3 justifying the SEM-EDS studies.

The characterization studies as discussed above give an account of the formation of different phases during the iron ore reduction process. The coconut shells burn off to generate hydrocarbons and carbon monoxide which act as the reducing gases in this process. The reduction at 800 °C is found to produce a good amount of magnetite, whereas at higher reducing conditions such as a temperature of 900 °C and a biomass to feed ratio of 0.3, feebly magnetite phases like wustite, fayalite and complex iron alumina silicates are formed justifying the drop of iron recovery to 25.77%. The over-reduction of magnetite to form wustite can be attributed to the burning of coconut shell at high temperature that enhances the reduction process. Similar observations have been made by researchers who have worked on the pyrolysis of biomass like wood and rice husk [29,30]. Similarly, the reactions between Fe_3O_4 and FeO with silica and alumina phases (Eqs. (1) and (2)) that leads to phases like fayalite (Fe_2SiO_4) become inevitable at higher temperature [31].

$$2Fe_3O_4 + 3SiO_2 \rightarrow 3Fe_2SiO_4 + O_2 \quad (1)$$

$$2FeO + SiO_2 \rightarrow Fe_2SiO_4 \quad (2)$$

The silica source required for the formation of fayalite is likely from quartz or the decomposition of kaolinite present in the ore [32]. It is noteworthy that the kaolinite present in the feed gives rise to silicate phases at 700 °C (Fig. 9-S1). However, these phases look more distinct and separable at 800 °C (Fig. 9-S2) that leads to better liberation and hence, better magnetic separation from the iron phases. At 900 °C, a majority of the iron values get associated with these silicate phases and report in the non-magnetic fraction seriously affecting the iron recovery of the magnetic product.

To gain further understanding of the mineral phases present in the magnetic and non-magnetic fractions of the optimum product (S2), the respective fractions were subjected to XRD, and the patterns are displayed in Fig. 11. The magnetic fraction shows the predominant occurrence of magnetite with a little amount of hematite (Fig. 11a), whereas the non-magnetic fraction (Fig. 11b) consists of hematite, maghemite, fayalite and corundum. It is to be noted that maghemite and corundum were not identifiable in the magnetite dominated roasted product of S2, probably due to their minimal presence below the detection level of XRD. Maghemite (γ-Fe_2O_3) has less magnetic

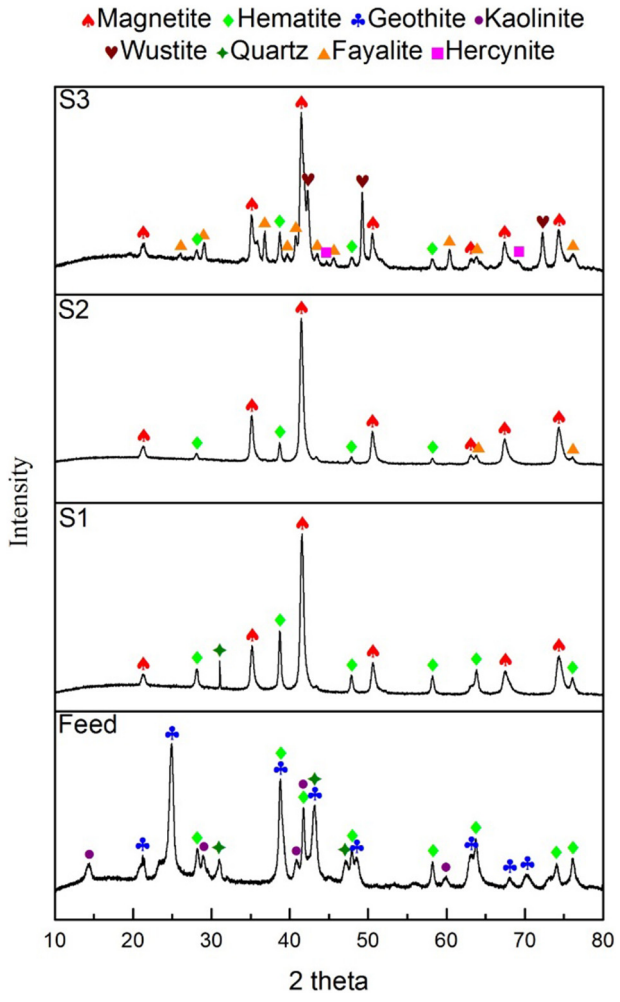

Fig. 10. XRD patterns of feed and reduced products.

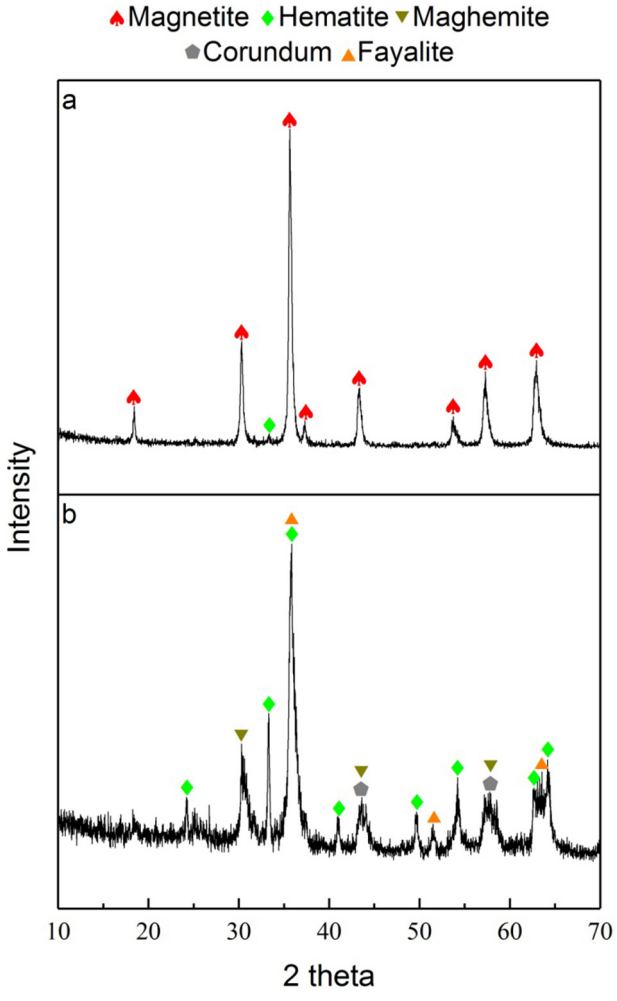

Fig. 11. XRD patterns of (a) magnetic and (b) non-magnetic fractions of the optimum roasted product S2.

properties than magnetite, but higher than hematite [33]. The presence of little maghemite in the non-magnetic fraction can be because of its close association with hematite or other phases. In the same way, the formation of corundum (Al_2O_3) may be because of the disintegration of kaolinite at high temperature [32].

3.3.3. Thermal behaviour

The TG profiles of CS and iron ore are shown in Fig. 12a. Each of the profile can be categorised into three different regions, namely Region I, Region II and Region III. The mass loss of 27% in Region I of the TG curve of CS refers to the removal of its free water and moisture content. This process continues up to 195 °C. The second stage (Region II) corresponds to the pyrolysis process of the biomass. In this region, it drastically loses weight until around 350 °C. After that, in Region III, the rate of pyrolysis is found to continue at a much slower rate. On the other hand, the TG profile of iron ore shows a slow rate of weight loss up to 250 °C in Region I. This could correspond to the removal of the free hydroxyl content in the iron ore samples. In Region II, a significant loss of weight occurs until 390 °C. The weight loss of iron ore in this region is 7%. It can be attributed to the dehydroxylation process of goethite (FeOOH) transforming it to hematite (Fe_2O_3), which is consistent with earlier results [34,35]. The weight loss continues up to 800 °C due to the decomposition of clay particles, as can be seen in Region III. This loss, in the present case, is around 2%.

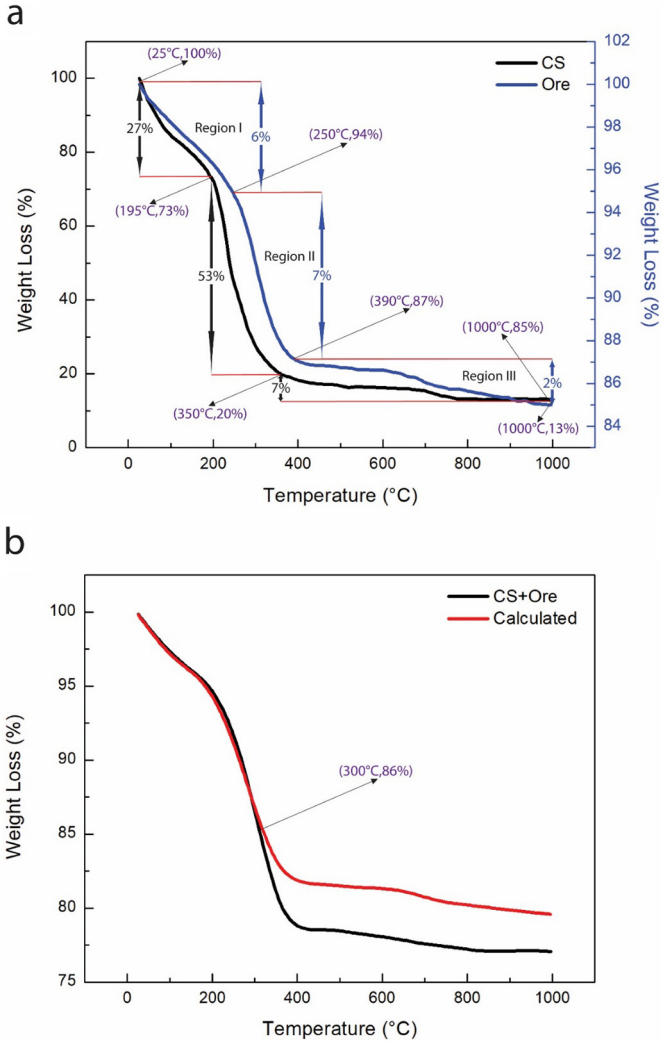

Fig. 12. (a) TG pattern of raw materials under inert gas atmosphere, and (b) comparison between the TG patterns of the experimental mixture and the calculated weighted sum.

The TG curve of the mixture (iron ore mixed with 20 wt% CS), as shown in Fig. 12b is compared with the calculated weighted sum, which is the sum of the individual weight loss data of iron ore and CS according to their weight percentages. It is depicted from the figure that the experimental data of the mixture is consistent with the calculated weight sum up to 300 °C. This suggests that there is hardly any interaction between the pyrolysis products of CS and the ore. The deviation of the experimental data from the calculated data is noticed when the temperature increases further. The data reveal that the reduction of iron ore starts from about 300 °C. This can be assumed to be facilitated by the gases and extra heat generated from the pyrolysis of hemicellulose and lignin that are the essential components of CS [36].

4. Conclusion

Reduction roasting is gaining importance considering most of the low-grade iron ores do not respond to physical separation processes owing to the poor liberation of the associated mineral phases. Recognizing the importance of the development and exploration of new alternatives to coal-based reductants, the present study has put forward a novel application of waste coconut shells in the reduction roasting of a goethitic iron ore overburden. Under optimum conditions, i.e., a temperature of 800 °C, a time of 60 min and a CS to feed ratio of 0.2, the overburden sample having 49% Fe could be upgraded to concentrate with 63.2% Fe at an iron recovery of 66.2%. With coconut shells being used as the reductant, the process is likely to address environmental issues by replacing coal and reducing the burden of dumping agricultural wastes as well as iron ore overburden.

Acknowledgements

The authors are thankful to the Director, CSIR-IMMT, Bhubaneswar for his kind permission to publish this paper. The authors are also thankful to the Ministry of Steel, Government of India for funding this work (Grant number: F. No. 11(12)/GBS/2014-TW).

References

[1] J.M.F. Clout, J.R. Manuel, 2 - Mineralogical, chemical, and physical characteristics of iron ore, in: L. Lu (Ed.), Iron Ore, Woodhead Publishing 2015, pp. 45–84, https://doi.org/10.1016/B978-1-78242-156-6.00002-2.
[2] M.A. Wells, R.W. Fitzpatrick, R.J. Gilkes, Thermal and mineral properties of Al-, Cr-, Mn-, Ni- and Ti-substituted goethite, Clay Clay Miner. 54 (2006) 176–194, https://doi.org/10.1346/CCMN.2006.0540204.
[3] N. Faris, J. Tardio, R. Ram, S. Bhargava, M.I. Pownceby, Investigation into coal-based magnetizing roasting of an iron-rich rare earth ore and the associated mineralogical transformations, Miner. Eng. 114 (2017) 37–49, https://doi.org/10.1016/j.mineng.2017.09.007.
[4] S.S. Rath, N. Dhawan, D.S. Rao, B. Das, B.K. Mishra, Beneficiation studies of a difficult to treat iron ore using conventional and microwave roasting, Powder Technol. 301 (2016) 1016–1024, https://doi.org/10.1016/j.powtec.2016.07.044.
[5] S.S. Rath, H. Sahoo, N. Dhawan, D.S. Rao, B. Das, B.K. Mishra, Optimal recovery of iron values from a low grade iron ore using reduction roasting and magnetic separation, Sep. Sci. Technol. 49 (2014) 1927–1936, https://doi.org/10.1080/01496395.2014.903280.
[6] X. Liu, H. Zhang, S. Li, D. Li, D. Huang, Research on reduction of Fe_2O_3 by biomass sawdust, J. Shanghai Jiaotong Univ. Sci. 22 (2017) 280–285, https://doi.org/10.1007/s12204-017-1833-5.
[7] K. Zhang, X. li Chen, W. chao Guo, H. juan Luo, Z. jun Gong, B. wei Li, W. fei Wu, Effects of biomass reducing agent on magnetic properties and phase transformation of Baotou low-grade limonite during magnetizing-roasting, PLoS One 12 (2017), e0186274. https://doi.org/10.1371/journal.pone.0186274.
[8] P. Salatino, R. Solimene, Mixing and segregation in fluidized bed thermochemical conversion of biomass, Powder Technol. 316 (2017) 29–40, https://doi.org/10.1016/j.powtec.2016.11.058.
[9] P. McKendry, Energy production from biomass (part 1): overview of biomass, Bioresour. Technol. 83 (2002) 37–46, https://doi.org/10.1016/S0960-8524(01)00118-3.
[10] V. Strezov, Iron ore reduction using sawdust: experimental analysis and kinetic modelling, Renew. Energy 31 (2006) 1892–1905, https://doi.org/10.1016/j.renene.2005.08.032.
[11] S. Yaman, Pyrolysis of biomass to produce fuels and chemical feedstocks, Energy Convers. Manag. 45 (2004) 651–671, https://doi.org/10.1016/S0196-8904(03)00177-8.

[12] W. Yong-bin, Z.H.U. Guo-cai, C.H.I. Ru-an, Z. Yu-na, C. Zhuo, An investigation on reduction and magnetization of limonite using biomass, Chin. J. Process. Eng. 9 (2009) 508–513.
[13] Y. Wu, M. Fang, L. Lan, P. Zhang, K.V. Rao, Z. Bao, Rapid and direct magnetization of goethite ore roasted by biomass fuel, Sep. Purif. Technol. 94 (2012) 34–38, https://doi.org/10.1016/j.seppur.2012.04.008.
[14] R.Z. Abd Rashid, H. Mohd. Salleh, M.H. Ani, N.A. Yunus, T. Akiyama, H. Purwanto, Reduction of low grade iron ore pellet using palm kernel shell, Renew. Energy 63 (2014) 617–623, https://doi.org/10.1016/j.renene.2013.09.046.
[15] Q. Wang, Y. Wu, Y. Li, X. Yang, Biomass reduction roasting-magnetic separation of low grade goethite, Mater. Sci. Forum 814 (2015) 235–240.
[16] S.S. Rath, D.S. Rao, A. Tripathy, S.K. Biswal, Biomass briquette as an alternative reductant for low grade iron ore resources, Biomass Bioenergy 108 (2018) 447–454, https://doi.org/10.1016/j.biombioe.2017.10.045.
[17] Statistics: Coconut Development Board, http://coconutboard.nic.in/stat.htm 2017, Accessed date: 14 February 2018.
[18] K. Yang, J. Peng, C. Srinivasakannan, L. Zhang, H. Xia, X. Duan, Preparation of high surface area activated carbon from coconut shells using microwave heating, Bioresour. Technol. 101 (2010) 6163–6169, https://doi.org/10.1016/j.biortech.2010.03.001.
[19] A.R. Hidayu, N. Muda, Preparation and characterization of impregnated activated carbon from palm kernel shell and coconut shell for CO_2 capture, Procedia Eng. 148 (2016) 106–113, https://doi.org/10.1016/j.proeng.2016.06.463.
[20] A. Anwar, S. Ahmad, S.A. Ahmed, Performance of waste coconut shell as partial replacement of natural coarse aggregate in concrete, Int. J. Sci. Eng. Res. 7 (2016) 1802–1809.
[21] B.H. Stuart, B. George, P. Mclntyre, Modern Infrared Spectrocopy, Second Wiley, England, 1996.
[22] A.-N.A. El-Hendawy, Variation in the FTIR spectra of a biomass under impregnation, carbonization and oxidation conditions, J. Anal. Appl. Pyrolysis 75 (2006) 159–166, https://doi.org/10.1016/j.jaap.2005.05.004.
[23] A.T. Mohd Din, B.H. Hameed, A.L. Ahmad, Batch adsorption of phenol onto physiochemical-activated coconut shell, J. Hazard. Mater. 161 (2009) 1522–1529, https://doi.org/10.1016/j.jhazmat.2008.05.009.
[24] T. Siengchum, M. Isenberg, S.S.C. Chuang, Fast pyrolysis of coconut biomass – an FTIR study, Fuel. 105 (2013) 559–565, https://doi.org/10.1016/j.fuel.2012.09.039.
[25] O. Faix, Classification of lignins from different botanical origins by FT-IR spectroscopy, Holzforsch. - Int. J. Biol. Chem. Phys. Technol. Wood. 45 (2009) 21–28, https://doi.org/10.1515/hfsg.1991.45.s1.21.
[26] C.-M. Popescu, M.-C. Popescu, G. Singurel, C. Vasile, D.S. Argyropoulos, S. Willfor, Spectral characterization of eucalyptus wood, Appl. Spectrosc. 61 (2007) 1168–1177, https://doi.org/10.1366/000370207782597076.
[27] L.M. Kline, D.G. Hayes, A.R. Womac, N. Labbe, Lignin determination in IL, BioResources. 5 (2010) 1366–1383.
[28] Z. Cui, Q. Liu, T.H. Etsell, Magnetic properties of ilmenite, hematite and oilsand minerals after roasting, Miner. Eng. 15 (2002) 1121–1129, https://doi.org/10.1016/S0892-6875(02)00260-1.
[29] Y. Hata, H. Purwanto, S. Hosokai, J. Hayashi, Y. Kashiwaya, T. Akiyama, Biotar ironmaking using wooden biomass and nanoporous iron ore, Energy Fuel 23 (2009) 1128–1131, https://doi.org/10.1021/ef800967h.
[30] H. Purwanto, N. Selamat, T. Akiyama Pramusanto, Pre-reduced iron produced from low grade ore using biomass, SEAISI Q. J. 39 (2010) 18–22.
[31] J.C. van den Berg, R.J. Dippenaar, Fluidized-bed reduction of fine iron ore by the in situ combustion of coal, J. South. Afr. Inst. Min. Metall. 89 (1989) 89–98.
[32] X. Liu, X. Liu, Y. Hu, Investigation of the thermal behaviour and decomposition kinetics of kaolinite, Clay Miner. 50 (2016) 199–210, https://doi.org/10.1180/claymin.2015.050.2.04.
[33] M. Gotić, G. Koščec, S. Musić, Study of the reduction and reoxidation of substoichiometric magnetite, J. Mol. Struct. 924–926 (2009) 347–354, https://doi.org/10.1016/j.molstruc.2008.10.048.
[34] G. Liu, V. Strezov, J.A. Lucas, L.J. Wibberley, Thermal investigations of direct iron ore reduction with coal, Thermochim. Acta 410 (2004) 133–140, https://doi.org/10.1016/S0040-6031(03)00398-8.
[35] Y. Wu, Y.H. Li, X. Yang, P. Zhang, Z.Y. Bao, The reduction mechanism of biomass roasting of goethite ores, Adv. Mater. Res. 560–561 (2012) 441–446, https://doi.org/10.4028/www.scientific.net/AMR.560-561.441.
[36] H. Yang, R. Yan, H. Chen, D.H. Lee, C. Zheng, Characteristics of hemicellulose, cellulose and lignin pyrolysis, Fuel. 86 (2007) 1781–1788, https://doi.org/10.1016/j.fuel.2006.12.013.